Proceedings of the ASME 2024 43nd International Conference on Ocean, Offshore and Arctic Engineering
OMAE2024
June 9-14, 2024, Singapore EXPO, Singapore

OMAE2024-127214

ANALYZING EXPERIMENTAL DATA OF 6-DOF MOTIONS AND SLOSHING IMPACTS IN LNG CARRIERS

Yangjun Ahn
Sungshin Women's University
Seoul, Korea

Mun-Gwan Choi
HD Hyundai Heavy Industries
Seongnam, Korea

Cheonjin Park
HD Hyundai Heavy Industries
Seongnam, Korea

Sang-Yeob Kim
Korean Register
Busan, Korea

Taehyun Park
Seoul National University
Seoul, Korea

Woohyeon Shim
Sungshin Women's University
Seoul, Korea

Gyeongbin Ryoo
Sungshin Women's University
Seoul, Korea

ABSTRACT

This research delves into the intricate relationship between the 6-degree-of-freedom (DoF) motion of LNG-related vessels and the sloshing impact loads. Conducted by HD Hyundai Heavy Industries, over a decade of sloshing model tests at Seoul National University's facility has led to a comprehensive study. The tests involve more than 30 ship models under 5,000 varied maritime conditions. A sophisticated array of over 100 Piezo electric sensors collect data on sloshing impact pressures, alongside the vessels' 6-DoF irregular motions, across five-hour test periods at real-ship scale. Post-processing utilizes the three-parameter Weibull distribution to extract the three-hour most probable maximum peak pressures as the sloshing loads from the time series data. Subsequently, the study examines the correlation between 18 features of the ship's 6-DoF motion—encompassing displacement, velocity, and acceleration—and the measured sloshing impact peak pressures. Machine learning techniques are pivotal in determining the significance of each feature, employing both linear and nonlinear analyses including Generalized Additive Models (GAMs). By using elimination methods based on the Light Gradient-Boosting Machine (LightGBM), the research identifies and elucidates the key parameters among the eighteen features that significantly influence sloshing loads. This comprehensive investigation not only deepens understanding of the intricate interplay between ship movements and sloshing impacts but also provides a useful dataset that could potentially inform future navigational strategies and contribute to enhancing safety and efficiency in maritime operations and hull form design.

Keywords: Sloshing; data mining; seakeeping; correlation; experiment; LightGBM; GAMs

1. INTRODUCTION

The estimation of sloshing impact loads has persistently posed a significant challenge to researchers engaged in the domains of fluid dynamics and naval motion [1, 2]. In the context of global efforts to curtail greenhouse gas emissions, a substantial number of marine vessels have transitioned to utilizing natural gas as a primary fuel source [3]. This shift has particularly influenced the design and operation of floating structures engaged in liquid cargo transportation, including natural gas carriers, which have undergone considerable enlargement to enhance operational efficiency. Notably, the standard size of natural gas carriers has escalated from 130k in the early 2000s to nearly 200k in recent constructions [4]. This escalation underscores the imperative of precise sloshing load estimation in the design phase of these vessels. It is particularly crucial to note that sloshing phenomena are intrinsically induced by the vessel's motion [5, 6], thereby necessitating a thorough analysis within the seakeeping study.

Conventionally, the estimation of sloshing impact loads is conducted through model testing due to the highly nonlinear nature of sloshing phenomena and the intricate interplay of multiple physical variables [2, 7]. Esteemed Korean institutions, including Hyundai Heavy Industries and the Korean Register, have consistently engaged in such model tests over extended periods to determine sloshing impact loads for integration into their design paradigms [8]. These entities have furthered their research endeavors grounded on a foundation of experimental data and insights amassed over a decade.

The present study employs experimental data to probe the dynamics interrelating ship motion and sloshing impact loads. An initial part of the study involves validating the linear and the

nonlinear correlation between ship motion and sloshing impact loads. Subsequently, a spectrum of nonlinear analytical methods is employed to decode the intricate relationship between the ship's 6-degree-of-freedom (6DoF) and the sloshing impact loads. In the second part, the Pearson correlation is used in the linear analysis, while in nonlinear analysis, the Spearman correlation, Kendall's tau correlation, Distance Correlation, and Generalized Additive Models (GAMs) are utilized. In the last part, an elimination approach is systematically applied to each of the 6DoF in sequence, with the objective of discerning the specific movements that significantly influence sloshing impact loads and the extent of their loads based on the Light Gradient-Boosting Machine (LightGBM).

The analysis results confirmed a strong correlation between acceleration among the 6DoF movements' displacement, velocity, and acceleration and the sloshing impact loads. It was also found that the sway motion, heave motion, and roll motion among the 6DoF components have strong correlations. Yaw motion and surge motion, on the other hand, exhibit weak correlations. Excluding some components of the 6DoF movements from the input features increase the accuracy of machine learning predictions.

2. METHODS

2.1 Database

The investigation scrutinized the correlation between the 6DoF of the ship and the sloshing loads using data derived from model experiments. Hyundai Heavy Industries had been conducting these model tests annually at the SNU Sloshing Model Testing Facility since 2011. The sloshing model tests were designed to simulate the ship's motion over a period equivalent to 5 hours in real ship scale, facilitating data acquisition. To date, Hyundai Heavy Industries had amassed a repository of over 4,000 experimental data sets, either autonomously or in collaboration with other entities. The vessels involved in these tests ranged from liquefied natural gas carriers (LNGC) to Floating Liquefied Natural Gas (FLNG), Very Large Ethane Carrier (VLEC), and other LNG related vessels. The tanks used for measuring sloshing impact loads predominantly included cargo holds and fuel tanks, with the ship's 6DoF varying based on specific motion characteristics, operational conditions, and tank configuration.

The experimental methodology adhered to the International Towing Tank Conference (ITTC) guidelines [9, 10]. The scale ratios of the model tests, as archived in the database, spanned from 1/30 to 1/50. Model test data using ambient air and water were extracted and utilized from the dataset. The Froude scaling was applied in the construction of model tanks and the establishment of experimental conditions. The models were crafted from transparent acrylic plates to ensure adequate thickness, more than 35 mm. Additionally, sloshing impact loads were quantified by installing pressure sensors on the wetted surface of the model, with data subsequently processed for comprehensive analysis [11, 12]. The pressure sensors were the KISTLER 211B5 model, which is an integrated circuit piezoelectric type. A sampling rate of 20 kHz was employed, complemented by a high-pass filter with a 200 ms cut-off period to mitigate thermal shock effects [13, 14]. The placement of pressure sensors primarily focused on areas anticipated to exhibit significant sloshing impact loads under given experimental conditions. Several examples of the model test were presented in Figure 1: an FLNG model [15], an LNGC model [16], and a one-row and a two-row LNG fuel tank model [17].

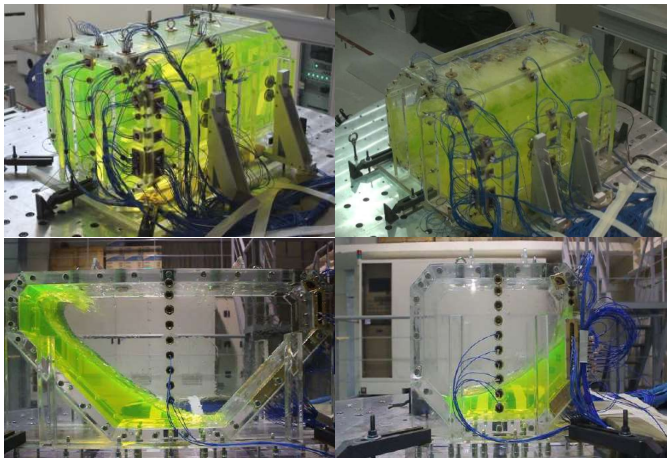

FIGURE 1: EXAMPLES OF MODEL TEST SNAPSHOTS: FLNG (TOP LEFT), LNGC (TOP RIGHT), ONE-ROW LNG FUEL TANK (BOTTOM LEFT), AND ONE-ROW LNG FUEL TANK (BOTTOM RIGHT)

2.2 6-DOF motions

For the experimental endeavors, the time series data representing the ship's 6DoF were generated based on linear motion theory. The wave-induced motions of the cargo hold model, denoted as ξ, were predicated upon linear theoretical principles. The simulation motions can be defined by

$$\xi(t) = \sum_{k=1}^{N} |H_k| A_k \cos\left(\omega_{k,e} t + \varepsilon_k + \phi_k\right) \qquad (1)$$

where $A_k = [2S_\eta(\omega_{k,e})\Delta\omega]^{1/2}$, and H_k, φ_k, $\omega_{k,e}$, and $S_\eta(\omega)$ denotes the linear transfer function, the motion phase, the wave encounter frequency, and the wave spectrum. Each of these components played a pivotal role in accurately characterizing the wave-induced motions within the specified linear framework, thereby facilitating a comprehensive understanding of the dynamic behavior of the cargo hold model under wave influence. HD Hyundai Heavy Industries employed commercial and reputable motion analysis software to create accurate linear transfer functions, which were then conveyed to the model testing facility. The study utilized over 200 wave components, which underwent random discretization to accurately represent the wave field. Additionally, the phases of these components were determined via a random selection process. The facility, in turn, crafts the 6DoF time series, taking into consideration the precise location of the tank designated for measuring sloshing impact loads.

The irregular time signals of a cargo hold's response were a manifestation of the vessel's inherent characteristics intertwined with prevailing environmental and operational conditions. It was imperative to consider the simulation time signal of the cargo hold's response to delineate the correlation between the severity of sloshing loads and the distinct characteristics of the vessels. These 6DoF irregular time signals of the simulation can be methodically transformed into displacement, velocity, and acceleration time signals via elementary differentiation. Subsequently, the standard deviations of these signals, denoted as σ_ξ, σ_v, and σ_a, were computed. These calculated standard deviations can be succinctly represented through spectral moments [18]. The spectral moments of the response, denoted as m_{ij}, are defined as follows:

$$m_{ij} = \int_0^\infty \omega^i \cdot S_\eta(\omega)|H(\omega)|^2 d\omega \tag{2}$$

where the subscript i represents the order of the moment, and j denotes each component of the 6DoF motion. It is noted that the standard deviation of the responses is directly correlated with the simple integration of the response spectrum over the frequency domain, ω. Consequently, the zeroth, second, and fourth moments, denoted as m_{0j}, m_{2j}, and m_{4j} respectively, can be represented as the variance of displacement time signals (σ_ξ^2), the variance of velocity time signals (σ_v^2), and the variance of acceleration time signals (σ_a^2). These spectral moments were instrumental in encapsulating the characteristics of the responses, which were in turn influenced by the intrinsic properties of the vessels, operating conditions, and the surrounding environmental conditions. These 18 spectral moments were the primary input features of the present study.

2.3 Sloshing impact loads

A standardized approach [10, 19] to post-processing was utilized, employing a peak-over-threshold technique with a specified 0.2 s time window and a 2.5 kPa threshold pressure [10, 11]. Subsequent to the acquisition of sloshing impact peak pressures, a process of post-processing for impulse peak pressures was initiated. During an impact event, the maximal impulse peak pressure was extracted from all installed sensors; these maximum pressures were then collated for each test iteration, which was conducted over a span of five hours in real scale. These collated maximum pressures were organized into a sample set. To ascertain the likelihood of occurrence of peak pressures within each test run's sample set, a three-parameter Weibull distribution was employed [2, 7, 8, 10, 11]. The cumulative probability function of this distribution can be defined by the location parameter (δ), scale parameter (β), and shape parameter (γ).

$$F(x) = 1 - \mathrm{e}^{-\left(\frac{x-\delta}{\beta}\right)^\gamma} \tag{3}$$

The estimation of these parameters was facilitated through the moment method, which aligned the first three model moments of mean, variance, and skewness with their corresponding sample moments, employing equations that incorporate the Gamma function Γ.

$$\mu = \beta\Gamma\left(1+\frac{1}{\gamma}\right) + \delta \tag{4}$$

$$\sigma^2 = \beta^2\left(\Gamma\left(1+\frac{2}{\gamma}\right) - \Gamma^2\left(1+\frac{1}{\gamma}\right)\right) \tag{5}$$

$$\gamma_1 = \frac{\Gamma\left(1+\frac{3}{\gamma}\right) - 3\Gamma\left(1+\frac{1}{\gamma}\right)\Gamma\left(1+\frac{2}{\gamma}\right) + 2\Gamma^3\left(1+\frac{1}{\gamma}\right)}{\left(\Gamma\left(1+\frac{2}{\gamma}\right) - \Gamma^2\left(1+\frac{1}{\gamma}\right)\right)^{3/2}} \tag{6}$$

Upon fitting the impulse peak pressures to the Weibull distribution, the most probable maximum pressure for a 3-hour duration can be calculated, representing sloshing impact loads as the target feature of the present study.

2.4 Correlations

The Pearson correlation coefficient, denoted as r, is a measure of the linear correlation between two variables X and Y, giving a value between -1 and 1 inclusive. It was defined as the covariance of the two variables divided by the product of their standard deviations. It can be represented as:

$$r = \frac{\sum_{i=1}^n (X_i - \bar{X})\left((Y_i - \bar{Y})\right)}{\sqrt{\sum_{i=1}^n (X_i - \bar{X})^2}\sqrt{\sum_{i=1}^n (Y_i - \bar{Y})^2}} \tag{7}$$

A value of 1 implies a perfect positive linear relationship, -1 implies a perfect negative linear relationship, and 0 implies no linear correlation between the variables. This coefficient is widely used in the fields of statistics, finance, and more due to its simplicity and clear interpretability [20].

Spearman's rank correlation coefficient, denoted r_s, is a nonparametric measure of rank correlation that assesses the strength and direction of association between two ranked variables [21]. It is a measure of how well the relationship between two variables can be described using a monotonic function. The formula for Spearman's rank correlation is given by:

$$r_s = 1 - \frac{6\sum d_i^2}{n(n^2-1)} \tag{8}$$

where d_i is the difference between the ranks of corresponding variables and n is the number of observations. Spearman's coefficient ranges between -1 and 1, with -1 indicating a perfect negative monotonic relationship and +1 indicating a perfect positive monotonic relationship [22].

Kendall's tau correlation coefficient, denoted as τ, is a measure that identifies the strength of the association between

two variables. It is particularly useful for data without assuming the normality of the variables. Kendall's tau is defined as:

$$\tau = 1 - \frac{2}{n(n-1)} \sum_{i<j} \operatorname{sgn}(x_i - x_j) \operatorname{sgn}(y_i - y_j) \quad (9)$$

where x_i and y_i are the values of the two variables at each observation, i and j are index variables, and sgn is the sign function. The coefficient values range between -1 (100% disagreement) and 1 (100% agreement). When the value is zero, it indicates that there is no association between the two variables. Kendall's tau is often preferred over Spearman's correlation when the data set is small and has many tied ranks [23].

Distance Correlation (dCor) is a nonparametric measure and adept at detecting both linear and nonlinear associations between two multivariate random variables or vectors, offering a more nuanced understanding of dependency compared to traditional correlation coefficients. The essence of distance correlation lies in its capacity to quantify statistical dependence through the calculation of distance matrices. The distance correlation R between two random vectors X and Y is defined as:

$$R(X,Y) = \frac{\mathrm{A}(X,Y)}{\sqrt{\mathrm{A}(X,Y) \cdot \mathrm{A}(X,Y)}} \quad (10)$$

Here, A(X, Y) represents the distance covariance between X and Y, while A(X,X) and A(Y,Y) denote the distance variances of X and Y, respectively, all computed using double-centered distance matrices [24]. The value of distance correlation ranges between 0 (indicating complete independence) and 1 (indicating a perfect dependent relationship), making it an intuitive and effective measure for unraveling the intricacies of inter-variable relationships in a wide array of scientific domains.

GAMs are a flexible class of regression models that extend generalized linear models (GLMs) by allowing non-linear functions of the predictor variables while maintaining additivity [25]. GAMs provide a powerful framework for modeling complex relationships without assuming a specific parametric form. The fundamental equation of a GAM is:

$$g\big(E(Y)\big) = \beta_0 + f_1(X_1) + f_2(X_2) + \cdots f_p\big(X_p\big) \quad (11)$$

where Y, $E(Y)$, g, β_0, X, and f are the response variable, the expected value of Y, a link function, the intercept, predictor variable, and the smooth function of X. The smooth function $fi(X_i)$ are estimated using cubic splines. The smoothness of the function is controlled by a smoothing parameter, which can be chosen through cross-validation to avoid overfitting. The effective degrees of freedom (EDoF) for a spline can be given as $trace(S)$, where S is the smoother matrix used to transform the input data into the smoothed data. The EDoF provides a measure of the model's complexity.

The final correlation analysis method employed is the elimination method. It assumes that the 6DoF of the ship motion are independent of other experimental factors, and all factors other than the 6DOF are held constant. Initially, the sloshing impact load is set as the target value, and the Light Gradient-Boosting method (LightGBM), one of the machine learning methods, is used to estimate this target based on the experimental factors [26]. Initially, the estimation accuracy is set based on considering all components of the 6DoF motion, including displacement, velocity, and acceleration. Then, items related to the 6DoF motion are eliminated one by one, and the same LightGBM method is applied to calculate the estimation accuracy. The results are compared with the baseline values, considering all components of the 6DoF motion, to identify combinations that significantly deviate from the baseline and to ascertain the importance of the eliminated components.

LightGBM is a well-known efficient gradient boosting framework that utilizes tree-based learning algorithms. Developed by Microsoft, it is designed for distributed and efficient training, particularly on large datasets. LightGBM improves upon the traditional gradient boosting method by employing a novel technique known as Gradient-based One-Side Sampling (GOSS) and Exclusive Feature Bundling (EFB), which collectively enhance the efficiency and accuracy of the model. The core principle of LightGBM is to construct a series of decision trees, where each tree is built to correct the mistakes of its predecessor. The model is updated iteratively, with each step designed to minimize a loss function L, which is a measure of the difference between the predicted and actual values. The update rule can be represented simply as:

$$\Theta_{t+1} = \Theta_t - \alpha \cdot \nabla L \quad (12)$$

Here, Θ_t represents the parameters of the model at iteration t, α is the learning rate, and $\bigtriangledown L$ is the gradient of the loss function. This process continues until a stopping criterion, such as a maximum number of trees or a minimum loss reduction, is met. LightGBM's innovative approach to handling large datasets and high-dimensional features, along with its capability to produce highly accurate models with reduced training times, makes it a popular choice among data scientists and researchers.

3. RESULTS AND DISCUSSION

3.1 Linear and nonlinear correlations

Firstly, the results of applying linear and nonlinear correlation analysis methods for each of the 6DoF motions' displacement, velocity, and acceleration were compiled. These are presented in Table 1. When analyzing the correlation between the 6DoF movements' displacement, velocity, acceleration, and the sloshing impact loads, all the methods used consistently showed relatively high correlation values for acceleration and velocity. A previous study demonstrated the displacement of 6DoF motions using different data sets [8], and the current results show similarities to those findings. Among the 6DoF movements, heave, sway, and roll exhibited a closer relationship compared to other movements. Yaw acceleration and surge displacement showed a very weak relationship in all

the applied analysis methods. According to the linear relationship analysis results, heave acceleration, heave velocity, and sway acceleration displayed strong relationships, while Spearman's correlation analysis showed a strong relationship for roll velocity. The results of Kendall Tau's correlation analysis additionally indicated a strong relationship for roll acceleration. The distance correlation analysis results showed that yaw velocity component had a relatively high correlation.

TABLE 1: COMPARISON OF CORRELATION ANALYSIS RESULTS OF PEARSON, SPEARMAN, KENDAL'S TAU, AND DISTANCE CORRELATION METHODS

Attribute	r	r_s	τ	R
m_{01}	0.0959	0.2219	0.1505	0.1541
m_{02}	0.2747	0.3686	0.2525	0.2794
m_{03}	0.2770	0.3480	0.2370	0.2921
m_{04}	0.2674	0.3581	0.2409	0.2865
m_{05}	0.1533	0.2689	0.1799	0.2261
m_{06}	0.2089	0.3339	0.2253	0.2710
m_{21}	0.1809	0.2654	0.1800	0.2121
m_{22}	0.3443	0.4238	0.2925	0.3489
m_{23}	0.3619	0.4244	0.2912	0.3751
m_{24}	0.2991	0.3781	0.2548	0.3012
m_{25}	0.1872	0.3039	0.2038	0.2670
m_{26}	0.2216	0.3541	0.2396	0.2965
m_{41}	0.1982	0.2744	0.1868	0.2484
m_{42}	0.3459	0.4517	0.3133	0.3873
m_{43}	0.3808	0.4711	0.3255	0.4214
m_{44}	0.2993	0.3765	0.2537	0.3039
m_{45}	0.1452	0.2668	0.1789	0.2342
m_{46}	-0.0336	0.2559	0.1705	0.1386

Next, the Generalized Additive Models (GAMs) method was employed to analyze the correlation between the sloshing impact loads and the 6DoF motions as input features. The analysis results of the GAMs are presented in Table 2.

EDoF values are highest for displacement and lowest for acceleration. This indicates that the complexity of displacement is greater than that of velocity or acceleration. In other words, it is difficult to directly correlate sloshing impact loads with displacement values, and it may be more appropriate to estimate sloshing loads using velocity or acceleration values. The *p*-value for testing the hypothesis that the predictor has no effect on the response indicates that yaw motion generally has a high *p*-value, suggesting that displacement, velocity, and acceleration of yaw motion are not significantly associated with sloshing impacts. A significance code (Sig. Code) based on the *p*-value provides a quick visual cue to the significance level, confirming that yaw motion displacement, velocity, and acceleration are not significantly associated with sloshing impact loads. In general, the vessel's 6DoF movement shows a more distinct association with sloshing impact loads through velocity and acceleration than through displacement.

A partial dependence plot derived from the GAMs are also obtained showing how the target variable is expected to change as the predictor changes. It is presented in Figure 2. In the partial dependence plots, each subplot corresponds to one predictor variable and its relationship with the sloshing loads as the target variable. The blue lines show the shape of the relationship between the predictor and the target variable. The red dashed lines confidence intervals around the shape of the relationship. They provide a range where the true function is expected to lie with a 95% level of confidence.

TABLE 2: ANALYSIS RESULTS OF GAMS

Attribute	EDoF	*p*-value	Sig. Code
m_{01}	13.4	1.28E-07	***
m_{02}	16.0	2.14E-04	***
m_{03}	15.2	5.80E-04	***
m_{04}	14.0	2.68E-03	**
m_{05}	15.0	1.88E-04	***
m_{06}	14.8	2.33E-02	*
m_{21}	9.0	7.48E-03	**
m_{22}	10.1	3.66E-05	***
m_{23}	13.0	1.05E-10	***
m_{24}	9.9	2.25E-11	***
m_{25}	12.1	3.57E-03	**
m_{26}	9.9	8.73E-04	***
m_{41}	4.1	1.19E-05	***
m_{42}	6.3	7.28E-08	***
m_{43}	4.1	2.33E-05	***
m_{44}	2.5	1.29E-04	***
m_{45}	5.7	2.35E-07	***
m_{46}	2.7	4.56E-03	**

The 6DoF movements' displacement, velocity, and acceleration exhibit a wide variety of relationships with the sloshing impact loads. Not only are the functional forms varied, but the levels of confidence and the sizes of the confidence intervals also differ, although certain commonalities can be identified as follows: The confidence intervals for velocity and acceleration are narrower than those for displacement. This supports the results previously confirmed through Pearson correlation, Spearman correlation, Kendall's tau correlation, and distance correlation. In other words, the 6DoF movements' velocity and acceleration show a relatively clear relationship with the sloshing impact loads. Among the 6DoF movements, heave and sway, in that order, have a closer relationship with the sloshing impacts. It is possible to make a more reliable estimation of sloshing loads using the heave and sway movements. Conversely, the yaw and the surge motions exhibit wide confidence intervals in certain sections.

Finally, the importance and relationships of input features were analyzed by applying the elimination method based on LightGBM. Firstly, the prediction error of mean squared error (MSE) considering all three aspects of the 6DoF movements' displacement, velocity, and acceleration was used as a baseline. Then, the results of predicting the sloshing loads were compared after sequentially removing input features related to the 6DoF movements. Model shapes and loading depth conditions unrelated to the 6DOF movements are included in all input

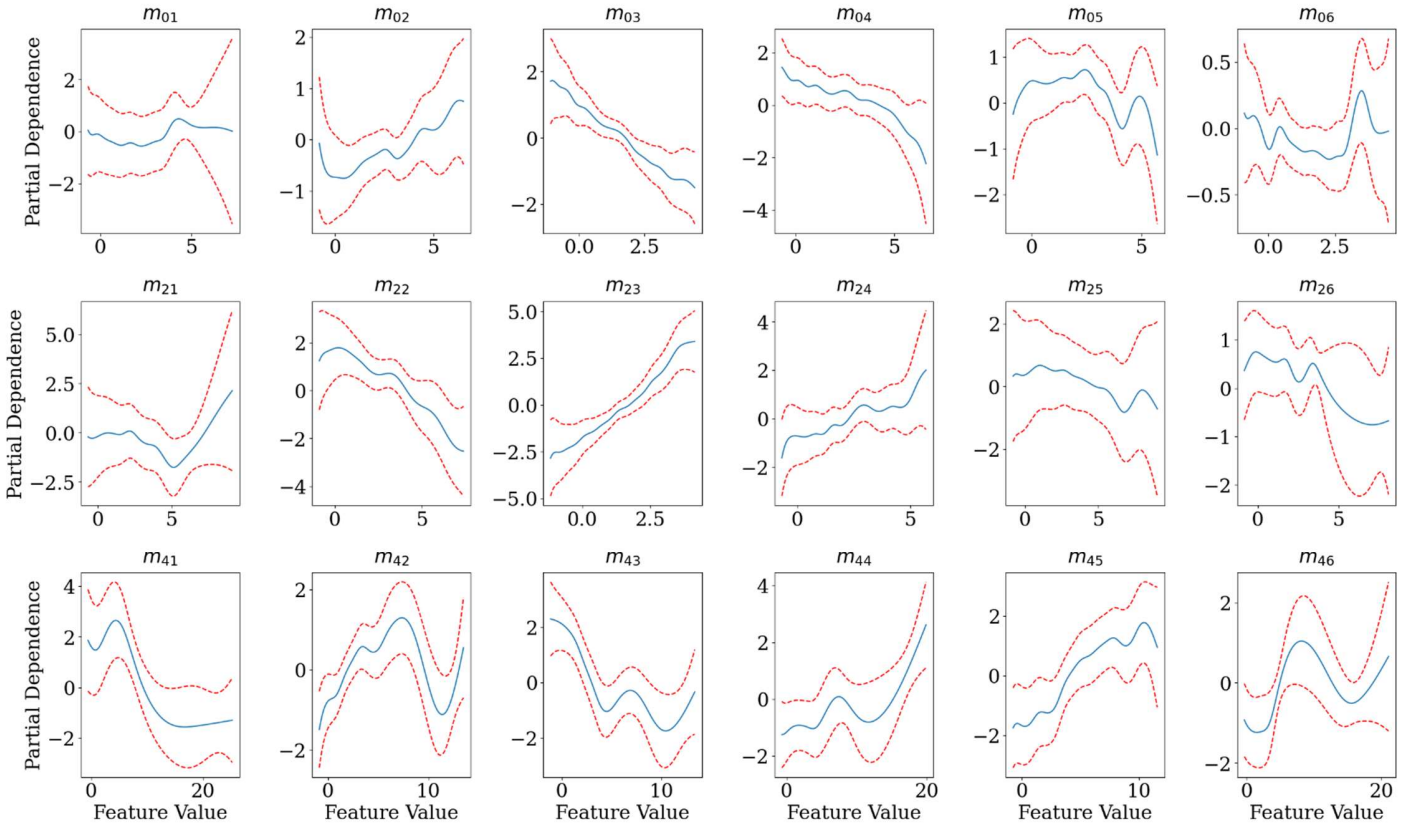

FIGURE 2: PARTIAL DEPENDENCE PLOT OF INPUT FEATURES DERIVED FROM GAMS.

features regardless of the elimination conditions. The conditions for the analysis applied with the elimination method are summarized in Table 3.

Initially, one or two terms of all 6DoF movements' displacement, velocity, and acceleration were removed. The elimination conditions are designated as C1, C2, C3, C4, C5, and C6. The terms that were not eliminated are referred to as C0, which is considered the baseline value, and this is concurrently represented as a straight line on the bar chart for comparison. These comparisons are presented in Figure 3. Most combinations of input features considering all 6DoF movements for displacement, velocity, and acceleration (C0) showed an increase in the error rate. However, when using the 6DoF movements of displacement and acceleration as input features, excluding velocity, the machine learning prediction error rate decreased. Additionally, it was observed that excluding the acceleration term significantly increased the error rate. This

TABLE 3: SUMMARY OF TEST CASES ELIMINATING INPUT FEATURES

Case	displacement	velocity	acceleration
C0	$m_{01,02,03,04,05,06}$	$m_{21,22,23,24,25,26}$	$m_{41,42,43,44,45,46}$
C1			$m_{41,42,43,44,45,46}$
C2		$m_{21,22,23,24,25,26}$	
C3	$m_{01,02,03,04,05,06}$		
C4		$m_{21,22,23,24,25,26}$	$m_{41,42,43,44,45,46}$
C5	$m_{01,02,03,04,05,06}$		$m_{41,42,43,44,45,46}$
C6	$m_{01,02,03,04,05,06}$	$m_{21,22,23,24,25,26}$	
C7	m_{01}	$m_{21,22,23,24,25,26}$	m_{41}
C8	m_{02}	$m_{21,22,23,24,25,26}$	m_{42}
C9	m_{03}	$m_{21,22,23,24,25,26}$	m_{43}
C10	m_{04}	$m_{21,22,23,24,25,26}$	m_{44}
C11	m_{05}	$m_{21,22,23,24,25,26}$	m_{45}
C12	m_{06}	$m_{21,22,23,24,25,26}$	m_{46}

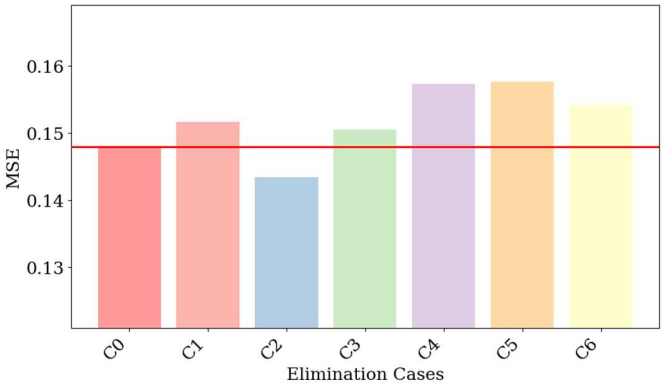

FIGURE 3: FIRST COMPARISON OF PREDICTION ERROR USING LIGHTGBM. DIFFERENT COMBINATION OF INPUT FEATURES ARE USED

supports the results from the previous correlation analysis, which confirmed that acceleration is closely associated with sloshing impact loads.

Based on the previous results obtained from applying the elimination method, better outcomes were achieved when terms related to velocity were excluded. Therefore, the velocity component of the 6DoF movements was fundamentally omitted, and the errors were compared by sequentially removing one of the 6DoF movements for displacement and acceleration. The prediction results of sloshing impact loads using LightGBM with the eliminated input feature combinations C7, C8, C9, C10, C11, and C12 can be summarized as follows: The prediction accuracy can be improved when machine learning is used after excluding the displacement and acceleration of surge motion, pitch motion, and yaw motion. Sway motion has a very close relationship with sloshing impact loads, and excluding it results in increased errors. Heave and roll motions do not have a significant impact. This is consistent with the results observed in the correlation analysis. The results are presented in Figure 4.

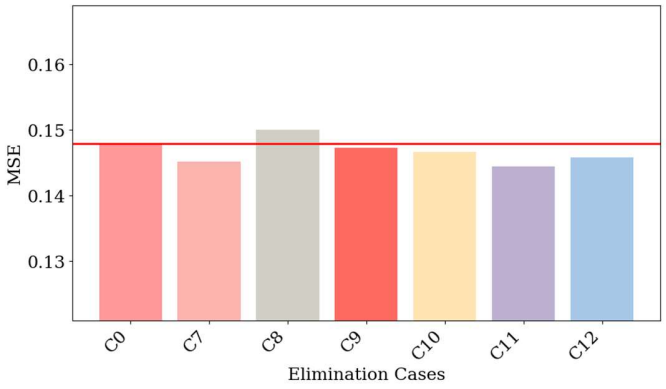

FIGURE 4: SECOND COMPARISON OF PREDICTION ERROR USING LIGHTGBM. DIFFERENT COMBINATION OF INPUT FEATURES ARE USED

4. CONCLUSIONS

Determining which of the ship's 6DoF movements significantly influences the sloshing impact load is an intriguing topic. If it is discovered that specific movements considerably affect the sloshing impact load, then during the design phase of the vessel, the vessel can be designed to mitigate these particular movements, thereby enhancing the stability. This information could also be valuable for developing autonomous ships, providing data that an agent could reference when seeking the optimal route. The results of examining the relationship between the ship's 6DoF movements and sloshing impacts using linear, nonlinear, and elimination methods are as follows:

- The 6DoF movements and sloshing impacts showed the strongest linear relationship with sway, heave, and roll movement, but generally, they are in a nonlinear relationship.
- Among the ship's displacement, velocity, and acceleration, acceleration has the most significant correlation on sloshing impact, and velocity has the least.
- The velocity of the 6DoF movements, as well as the displacement and acceleration of surge and yaw motions, are insignificantly associated with sloshing impact loads. Excluding these components could lead to improved efficiency when predicting sloshing impact loads using machine learning.

The following contents represent aspects that were challenging to address in the present study and require further research in the future.

- The relationship between the 6DoF movements and other experimental factors was assumed to be independent, and their mutual influence was not elucidated.
- The sloshing load was limited to impact pressure, and structural impacts were not considered.
- The results are based solely on experimental data, so various uncertainties related to experiments, such as convergence and scale ratio, exist. Realistically challenging, further validation using actual ship data is necessary.

ACKNOWLEDGEMENTS

This work was supported by Korean Register and HD Hyundai Heavy Industries. This work also supported by the National Research Foundation of Korea (NRF) grant funded by the Korea government (MSIT) (No. RS-2022-00166525). Their supports are highly appreciated.

REFERENCES

[1] S. Ji, H. Huang, X. Chen, J. Liu, X. Chen, Numerical and experimental analyses of a partially water-filled inclined floating body, Journal of Offshore Mechanics and Artic Engineering 145(6) (2023) 061202.

[2] S. Malenica, L. Diebold, S.H. Kwon, D.S. Cho, Sloshing assessment of the LNG floating units with membrane type containment system where we are?, Marine Structures 56 (2017) 99–116.

[3] Y. Choi, J. Ahn, C. Jo, D. Chang, Prismatic pressure vessel with stiffened-plate structures for fuel storage in LNG-fueled ship, Ocean Engineering, 196 (2020) 106829.

[4] B. Park, J. Jung, D. W. Jung, I. Park, S.-K. Cho, H.-G. Sung, Study on the estimation methods of roll damping coefficients using designed excitation device for harmonic roll motion, Proceedings of the 28th International Ocean and Polar Engineering Conference, Sapporo, Japan , 2018.

[5] Faltinsen and Timokha, Sloshing, Cambridge University Press, 2009.

[6] J.-F. Igbadumhe, M. Fürth, Hydrodynamic Analysis Techniques for Coupled Seakeeping–Sloshing in Zero Speed Vessels: A Review, Journal of Offshore Mechanics and Artic Engineering 143(2) (2021) 061202.

[7] M. Graczyk, T. Moan, Structural Response to Sloshing Excitation in Membrane LNG Tank, Journal of Offshore Mechanics and Artic Engineering 133(2) (2011) 021103.

[8] Y. Ahn, Y. Kim, S.-Y. Kim, Database of model-scale sloshing experiment for LNG tank and application of

artificial neural network for sloshing load prediction, Marine Structures (2019) 66-82.
[9] ITTC, ITTC Quality System Manual – Recommended Procedures and Guidelines – Sloshing model test, Rev. 01, 2021.
[10] S.-Y. Kim, Y. Kim, K.-H. Kim, Statistical analysis of sloshing-induced random impact pressures, Journal of Engineering and Maritime Environment 228 (2014) 235–48.
[11] DNV, Sloshing anlaysis of LNG membrane tanks, DNVGL-CG-0158, 2016.
[12] M. Graczyk, T. Moan, O. Rognebakk, Probabilistic analysis of characteristic pressure for LNG tanks, Journal of Offshore Mechanics and Artic Engineering 128(2) (2006) 133-144.
[13] B. Fillon, J. Henry, E. Baudin, L. Diebold, G. Parmentier, Q. Derbanne, Influence of sampling rates on sloshing pressures prediction, Proceedings of the 22nd International Ocean and Polar Engineering Conference, Rhodes, Greece 2012.
[14] S.-Y. Kim, K.-H. Kim, Y. Kim, Comparative study on pressure sensors for sloshing experiment, Ocean Engineering 94 (2015) 199–212.
[15] M.H. Oh, J.M. Kim, J.S. Moon, W.S. Sim, H.S. Shin, Sloshing assessment of FLNG cargo containment system due to sloshing loads in bimodal seas: effect of wave intensity, International Journal of Offshore and Polar Engineers 25 (2015) 170-177.
[16] S.-Y. Kim, Y. Kim, J. Lee, Comparison of sloshing-induced pressure in different scale tanks. Ships Offshore Structures 12 (2017) 244-261.
[17] J. Kim, S.-Y. Kim, Y. Kim, Experimental study of slosh-induced loads on LNG fuel tank of container ship, Proceedings of the 27th International Ocean and Polar Engineering Conference, CA, USA, 2017.
[18] A. Mansour, L. Donald, The principles of naval architecture series: strength of ships and ocean structures, 2010.
[19] M. Graczyk, and T. Moan, A probabilistic assessment of design sloshing pressure time histories in LNG tanks, Ocean Engineering 35 (2008) 834-855.
[20] B. Jacob, C. Jingdong, H. Yiteng, C. Israel, Pearson correlation coefficient, Noise Reduction in Speech Processing, Springer Topics in Signal Processing (STSP, 2) (2009) 1-4.
[21] L. Myers, M. J. Sirois, Spearman correlation coefficients, differences between, Encyclopedia of statistical sciences, Wiley Online Library, 2004.
[22] J. Hauke, T. Kosswski, Comparison of values of Pearson's and Spearman's correlation coefficients on the same sets of data, 30(2) (2011) 87–93.
[23] M. G. Kendall, A new measure of rank correlation, Biometrika, 30 (1/2) (1938) 81-93.
[24] G.J. Székely, M.L. Rizzo, N.K. Bakirov, Measuring and testing dependence by correlation of distances, Ann. Statist. 35(6) (2007) 2769 - 2794.
[25] T. Hastie, R. Tibshirani, Generalized Additive Models, Statistical Science, 1(3) (1986) 297-310.
[26] G. Ke, Q. Meng, T. Finley, T. Wang, W. Chen, W. Ma, Q. Ye, T.-Y. Liu, LightGBM: A highly efficient gradient boosting decision tree, Advances in Neural Information Processing Systems (2017) 30.